Hierarchically Organized Bimolecular Ladder Network Exhibiting Guided One-Dimensional Diffusion

Younes Makoudi,[†,∥] Emmanuel Arras,[†,∥] Nenad Kepčija,[†] Wolfgang Krenner,[†] Svetlana Klyatskaya,[‡] Florian Klappenberger,[†,*] Mario Ruben,[‡,§] Ari Paavo Seitsonen,[⊥] and Johannes V. Barth[†]

[†]Physik Department E20, Technische Universität München, James-Franck Strasse, 85748 Garching, Germany, [‡]Institute of Nanotechnology, Karlsruhe Institute of Technology, 76021 Karlsruhe, Germany, [§]IPCMS-CNRS UMR 7504, Université de Strasbourg, 23 Rue du Loess, 67034 Strasbourg, France, and [⊥]Physikalisch-Chemisches Institut der Universität Zürich, Winterthurerstr. 190, CH-8057 Zürich, Switzerland. [∥]These authors contributed equally to this work.

ABSTRACT

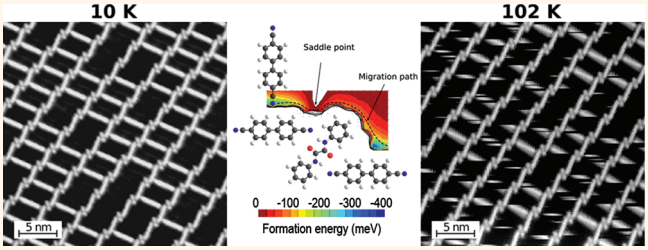

The assembly and dynamics of a hierarchical, bimolecular network of sexiphenyl dicarbonitrile and *N,N′*-diphenyl oxalic amide molecules on the Ag(111) surface are studied by scanning tunneling microscopy at controlled temperature. The network formation is governed by a two-step protocol involving hierarchic interactions, including a novel carbonitrile—oxalic amide bonding motif. For temperatures exceeding ∼70 K, more weakly bound sexiphenyl dicarbonitrile molecules carry out one-dimensional diffusion guided by the more stable substructure of the network held together by the carbonitrile—oxalic amide bonding motif. A theoretical investigation at the *ab initio* level confirms the different binding energies of the two coupling motifs and rationalizes the network formation and the diffusion pathway.

KEYWORDS: supramolecular chemistry · self-assembly · molecular dynamics · hierarchic bonding · scanning tunneling microscopy (STM) · density functional theory (DFT)

Molecular self-assembly is ubiquitous in biological systems for the production and reproduction of functional units and even living species.[1,2] Among the most important requirements for the formation of the highly complex supramolecular architectures is the presence of hierarchy in the bonding to allow multilevel assembly.[3] Adapting this strategy and creating novel molecular building blocks with the ability to self-assemble into supramolecular networks is a promising bottom-up technique in nanotechnology.[4−7] Many studies show examples of artificial self-assembled molecular nanostructures; however, they are often limited to only one level of order. Increasing efforts are dedicated to master the formation of ordered structure comprising a multilevel hierarchy.[8−12] At each level of organization, novel functionalities can be expected to be realized.[13] For further improvement of the control over the resulting architecture, hierarchy has to be introduced in the bonding motifs itself.[14,15]

Here we show a bimolecular two-level hierarchic assembly process which leads to a ladder-shaped two-dimensional (2D) network exhibiting intriguing dynamic behavior. In contrast to other heteromolecular approaches,[16−21] the two organic species couple *via* two distinct bonding motifs of different strength leading to a 2D supramolecular architecture consisting of two sublattices. The stronger bound sublattice is organized and linked by a novel hydrogen bond motif. At elevated temperature, the one-dimensional (1D) diffusion of the molecules of the weaker bond sublattice is guided by the more stable bimolecular grating.

RESULTS

The two molecules used in this study, namely, sexiphenyl dicarbonitrile (6DC) and *N,N*-diphenyl oxalic amide (DOA), are presented in Scheme 1. They were deposited from a double organic molecular beam epitaxy source onto a prepared Ag(111) substrate. Subsequent scanning tunneling microscopy (STM) observations were performed at a substrate temperature (T_{sub}) as indicated, typically 10 K. Both organic species have separately been the subject of detailed studies regarding their behavior on Ag(111) or Au(111) substrates.[22,23] It appears that DOA molecules (a) self-assemble into

* Address correspondence to florian.klappenberger@tum.de.

Received for review October 12, 2011 and accepted December 8, 2011.

Published online December 08, 2011
10.1021/nn203963a

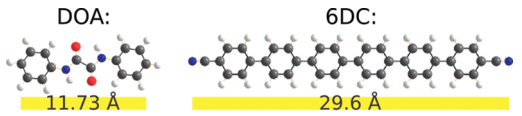

Scheme 1. Molecular building blocks used: *N,N′*-diphenyl oxalic amide (DOA), sexiphenyl dicarbonitrile (6DC). Hydrogen in white, carbon in black, oxygen in red, and nitrogen in blue.

hydrogen-bonded 1D molecular wires.[22,24] 6DC on the other hand (b) is found to arrange into a variety of highly regular, commensurate, and porous networks with various symmetries.[23,25]

As both molecules (6DC and DOA) are co-deposited on the Ag(111) surface, a different open-porous network arises, as shown by STM observation reported in Figure 1. The ratio of 6DC to DOA molecules is just under 2:1 in our experiments (63% 6DC and 37% DOA in Figure 1). The DOA molecules appear as two lobes and are shorter than the 6DC molecules which look like elongated sticks. The network consists of a series of 6DC−DOA chains ($6DC_{ch}$ and DOA aligned vertically in Figure 1), which are connected by brighter 6DC molecules that can be seen as rungs ($6DC_{ru}$), making it reminiscent of ladders. The pore size of the rhombic cavities (highlighted by the yellow area) is approximately equal to 7 nm^2. When all rungs of the ladders are present, the ratio 6DC to DOA is exactly 2:1. However, we observe here that the number of $6DC_{ru}$ spacers between the different lines is variable and depends on the coverage of 6DC, thus impacting the density of rhombic cavities. Dimensions relevant to the ladder network are drawn in yellow in Figure 1, including angles α, β, γ, δ, and ε of the different units with respect to the highlighted substrate direction and the periodicities A and B of the network along two directions. Measured values are $\alpha = 15.7°$, $\beta = 67.8°$, $\gamma = 85.5°$, $\delta = 1.8°$, $\varepsilon = 42.0°$, $A = 33.3$ Å, $B = 42.1$ Å.

The ladder-shaped supramolecular structure exhibits chiral properties which result from the heteromolecular binding motif as indicated in lower coverage data of Figure 2a. The STM image displays bimolecular chains that appear in five different directions (out of six observed in total) and can be classified in two enantiomeric variants (*Right* and *Left*). The analysis of all our data demonstrates that the two enantiomorphs are evenly present in the samples and that the supramolecular chain formation is controlled by the substrate periodicity. In addition, the energetic hierarchy behind the different bonds possible with the two organic species (Figure 2b) becomes evident. In the network, we could already distinguish two different interactions: $6DC_{ch}$−$6DC_{ru}$ and $6DC_{ch}$−DOA. Both of them involve the carbonitrile moiety of the 6DC molecule. The $6DC_{ch}$−$6DC_{ru}$ interaction is well-known from earlier work[23] and involves a C−N···H−C_{ph} binding motif. The 6DC−DOA interaction on the other hand was not observed prior in the self-assembly and will be discussed in more detail later. The last possible interaction, namely, DOA−DOA, is not present in the ladder network but appears in sample with excess DOA, as shown in Figure 2a. We can deduce from this that the 6DC−DOA interaction is stronger than the mean value of 6DC−6DC and DOA−DOA interactions.

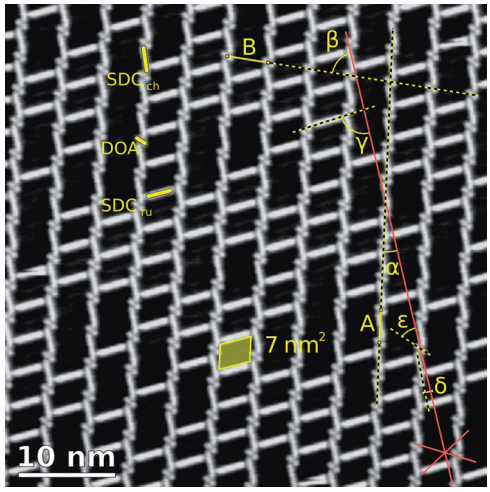

Figure 1. Overview STM topographic image of an open-porous network obtained after co-deposition of sexiphenyl dicarbonitrile ($6DC_{ch}$ and $6DC_{ru}$) and *N,N*-diphenyl oxalic amide (DOA) molecules on the Ag(111) surface. The substrate high-symmetry directions are marked by the red star (bottom right corner), also in all of our images. The different angles of the molecular units with respect to the indicated direction are noted α, β, γ, δ, and ε. The periodicity in two different directions is defined by lengths A and B (bias voltage $V_B = -1$ V, tunneling current $I = 70$ pA, substrate temperature $T_{sub} = 10$ K).

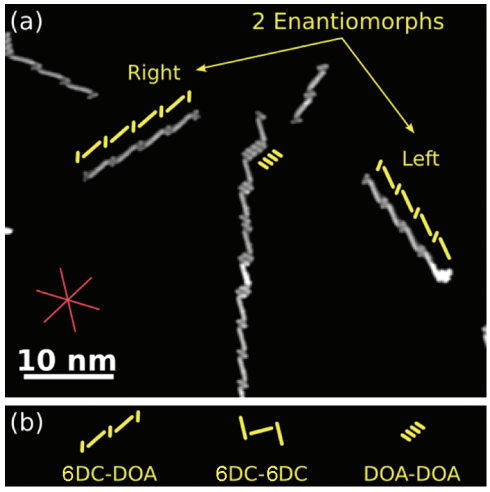

Figure 2. (a) STM topographic image of the chiral bimolecular chains at low coverage featuring the two enantiomorphs, *Right* and *Left* ($V_B = -1.16$ V, $I = 80$ pA, $T_{sub} = 10$ K). (b) Three types of bonds observed: 6DC−DOA, 6DC−6DC, and DOA−DOA. The preferred formation of alternate 6DC and DOA chains proves that the 6DC−DOA interaction is stronger on average than that between identical molecules (namely, 6DC−6DC and DOA−DOA).

DISCUSSION

For a better understanding of the novel binding motif, we start with the construction of a detailed

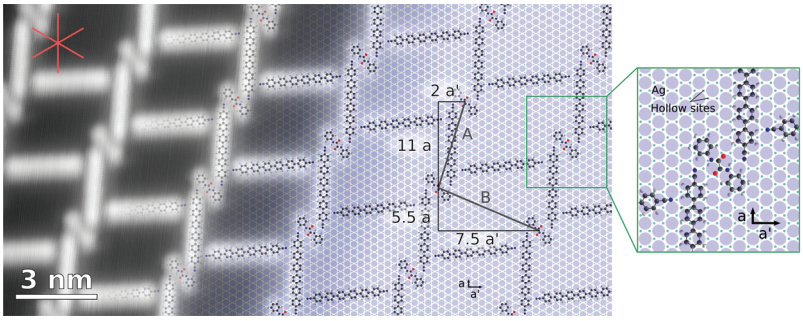

Figure 3. High-resolution STM data of the bimolecular open-porous network, superimposed with a ball-and-stick model of the molecules over the Ag(111) substrate. The original STM image has been geometrically corrected (shear and expansion ~3%) to better fit the model. Major characteristics of the network are indicated in substrate lattice parameter scale *a* and *a*′. The zoomed area highlights the position of molecules over the Ag substrate, where hollow sites are marked with small green dots (V_B = −1.12 V, I = 60 pA, T_{sub} = 10 K).

model of the network. The apparent height of the two molecules in our STM images (~1 Å, slightly depending on the tunneling conditions) is consistent with reported values for π-conjugated organic molecules in planar adsorption geometries.[26−30] Therefore, as a starting point, we considered only the flat conformations of both molecules to build our model displayed in Figure 3. To derive this model, three different approaches were combined: (i) a thorough analysis of numerous STM images, especially regarding the measurement of angle α and δ, as well as the angle between 6DC−DOA chains of two different chiralities (as seen for example in Figure 2a); (ii) the placement of the N atoms of 6DC molecules at hollow sites of the Ag(111) surface, as exposed in previous publications;[23,31] (iii) the detailed understanding of bonding regions as unraveled by theoretical calculations presented below. With this approach, it was possible to create an accurate model which fits (within usual STM error) all of our images, including the most peculiar configurations, such as near step edges (not shown here). This model, detailed in units of the Ag(111) surface in Figure 3, is confronted to a high-resolution STM image of the network and allows a very accurate evaluation of dimensions reported in Figure 1. The theoretical values thus are α = 17.5°, β = 67.1°, γ = 84.4°, δ = 1.6°, ε = 41.4°, A = 33.16 Å, B = 40.56 Å. These appear to be within 2° and 4% of the measured ones, well within the usual STM errors. The zoomed region of Figure 3 shows the substrate registry of our proposed model.

To further study the relative strength of the observed bonding motifs, we performed a series of experiments at different temperatures and evaluated the stability of the self-assembled structure. At T_{sub} = 75 K, we observe (Figure 4a) that $6DC_{ru}$ spacers start to move along the bimolecular chains. This result corroborates that the $6DC_{ch}$−$6DC_{ru}$ interaction is weaker than that for the $6DC_{ch}$−DOA. When the temperature of the substrate is increased to 102 K (Figure 4b), all $6DC_{ru}$ spacers diffuse but remain confined between $6DC_{ch}$−DOA chains. At 119 K (Figure 4c), the diffusion is even faster, but still the $6DC_{ch}$−DOA chains remain intact. They finally break at temperatures higher than 132 K (not shown).

Further analysis of similar images at nine different temperatures allowed us to draw the Arrhenius plot presented in Figure 4d. Specifically, as in a previous publication,[31] the hopping rate R is calculated using the expression $R = h_e/(h_p t)$, where h_e is the number of hopping events occurring during the time t, and h_p is the number of hopping-able 6DC molecules, that is, the molecules that have enough space to perform a movement. At low temperatures, t is the time elapsed between two successively taken pictures. For temperatures exceeding 103 K, as the hopping process is more frequent, only single pictures are analyzed, and h_e is evaluated for each molecule by counting the number of bright-to-dark and dark-to-bright changes in the $6DC_{ru}$ species (see Figure 4b,c), and t is the time necessary to scan enough lines to visualize the whole molecule. The best fit of these values gives an effective hopping barrier of 205 meV (±11 meV) and a prefactor of $2.7 \times 10^{9.4\pm0.6}$ Hz, well within the known broad range in the literature.[29,31,32]

Finally, it needs to be emphasized that the ladder rungs have a stabilizing effect on the separation of the $6DC_{ch}$−DOA chains. Interestingly, this holds even in the dynamic regime. From Figure 4b,c, it is evident that the $6DC_{ch}$−DOA chains form a highly regular grating whose periodicity is perfectly retained and unaffected after the onset of rung diffusion. Thus there is a dynamic stabilization of the supramolecular arrangement, which effect could be used in itself by using dicarbonitrile or other linkers with appropriate length or even other hierarchic bonding patters to fabricate tailored superlattices with definite regularity. By contrast, previously reported related 1D supramolecular gratings without stabilizing elements on a homogeneous surface inevitably showed a certain degree of variation in the distances between the constituting molecular lines,[33,34] even in the presence of

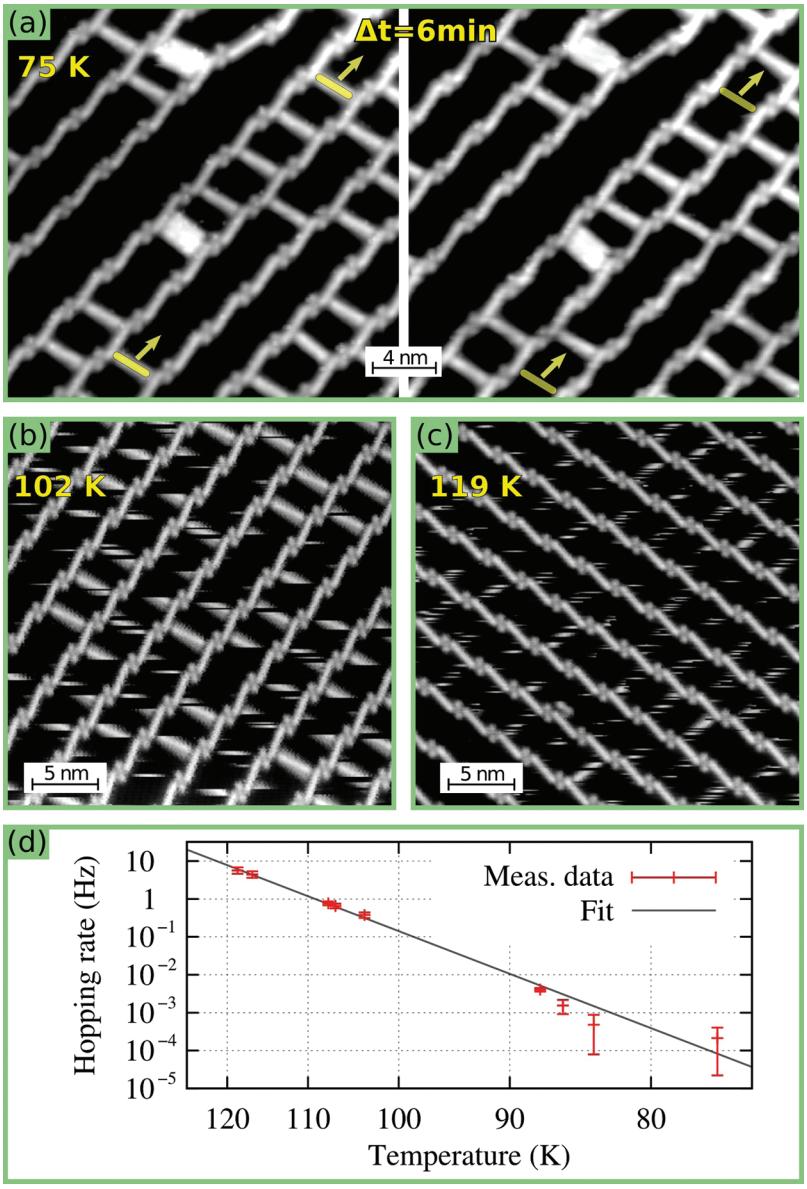

Figure 4. One-dimensional 6DC diffusion guided by the bimolecular chains: (a) T_{sub} = 75 K, the two images show the same area of the network (*Right* chirality), the second being taken 6 min after the first one. Arrows are added to highlight the hopping events. (b) T_{sub} = 102 K. Frizzled appearance of $6DC_{ru}$ indicates diffusion within stable chains. (c) T_{sub} = 119 K, *Left* chirality. The change in the frizzled features results from a higher hopping rate. (d) Arrhenius plot drawn from similar images at nine different temperatures. Data are corrected to take into account the low scanning speed of the STM at high hopping rates (temperatures). The derived least-squares fit gives an effective hopping energy of 205 ± 11 meV and a prefactor of $10^{9.4\pm0.6}$ Hz.

adatoms between them.[35] Thus, the introduction of the stabilizing effect by lateral weak linkages in hierarchic assemblies complements previous approaches with molecular gratings based on anisotropic templates.[19,36]

Theoretical Investigation. In order to better understand the nature of the 6DC−DOA interaction, as well as to quantitatively compare it to the $6DC_{ch}$−$6DC_{ru}$ bond, we performed total energy calculations within the density functional theory framework. The aim is not only to get the binding energies of the different bonds but also to have a clear picture of the complete energy landscape in the different binding regions of the molecules. Since this requires extensive computations, we tried to reduce as much as possible the computational cost of each. First, the simulations were performed without the presence of a substrate, as successfully used in a previous study.[37] By doing so, we assume that the interplay between the substrate−molecule and molecule−molecule bondings is minimal, which was checked with a test model, reported in the Supporting Information. Furthermore, this also allows us to study solely the interaction between molecules and not with the substrate. Finally, we have used the smaller NC−Ph_2−CN (biphenyl dicarbonitrile 2DC) molecule when only the CN group was involved

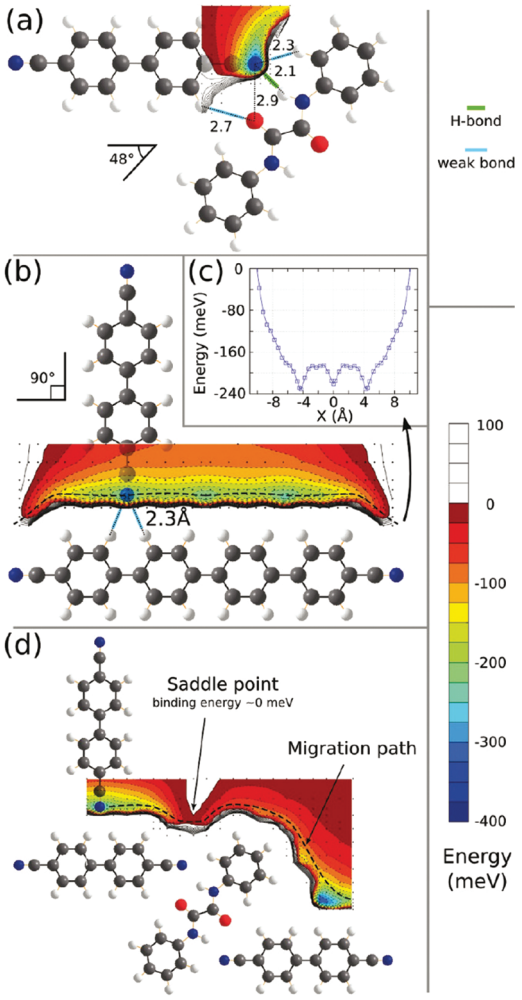

Figure 5. Energy maps of the three studied binding regions. Each black dot on the maps (more than 450 in total) is one simulation of rigidly displaced molecules and gives the position of the binding nitrogen atom. Colored areas of the interpolated full energy maps correspond to negative formation energy, hence binding zone, while positive formation energy areas are white. Isolines mark 25 meV steps. Dark green lines mark classical hydrogen bonds, whereas light blue ones highlight weak attractive interaction. (a) Binding of NC−Ph_2−CN (2DC) with DOA. (b) Binding of 2DC with 4DC. (c) Evolution of the formation energy *versus* translation along the 4DC ladder component. (d) Migration region around the 2DC−DOA−2DC link.

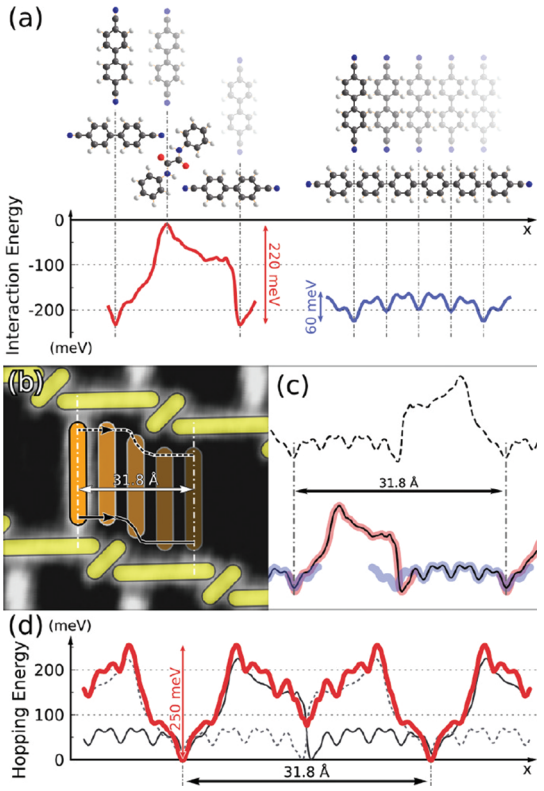

Figure 6. Prospective study of the migration path of $6DC_{ru}$ between two $6DC_{ch}$−DOA chains. (a) Computation of the interaction energy along the two parts of migration path: the step and the straight part. (b) Migration path drawn from a STM picture, namely, the simple translation of the $6DC_{ru}$ along the $6DC_{ch}$−DOA chain guides. (c) Reconstruction of the interaction energy along the full migration path for each side. (d) Sum of both contributions, plotted with respect to the stable state energy. The effective hopping energy barrier is 250 meV.

in the bonding motif. Extensive convergence tests of NC−Ph_X−CN molecules with the number of phenyl rings X up to 4 have indeed shown that the behavior of the CN group depends only weakly on X for $X > 2$.

The energy maps shown in Figure 5 were obtained *via* the following steps: (i) each molecule is first geometrically relaxed individually, as in the gas phase; (ii) two or more molecules are placed in various relative positions and the total energy of the resulting box is computed as is, without geometrical relaxation; (iii) the binding energy (in each configuration) is extracted by subtracting the total energy of the isolated constituting molecules; (iv) results are presented as energy maps (Figure 5), with colored (respectively white) areas corresponding to bonding (respectively antibonding) configurations and isolines for improved readability.

The first result (Figure 5a) is the binding energy map of a 2DC with a DOA. The angle of 48° between the 2DC and the DOA was derived from a previous full minimization revealing this equilibrium angle. We find that the binding energy reaches 340 meV at its maximum. In this equilibrium configuration, the closest distance between N and H atom is 2.1 Å (green thick line in Figure 5a). It is interesting to note that three interactions contribute to this link: CN···HN, CN···HC_{ph}, and C_{ph}H···OC. The first one is a classical hydrogen bond. The two others will be simply referred to as weak bonds[38] (blue thin lines in Figure 5). We evaluated the contribution of each bond in two steps. First, the binding energy of the configuration in Figure 5a was computed with the carbonitrile group of the 2DC replaced by a simple hydrogen. It was found to be ~70 meV and corresponds to the contribution of the C_{ph}H···O bond. Then, looking at the shape of the initial energy map, especially when the carbonitrile group is next to the HC_{ph} group and relatively far from the HN group,

we conclude that the CN···HN and CN···HC_{ph} bonds contribute up to 180 and 90 meV, respectively. Thus, we can infer that the binding between a 2DC and a DOA comprises a 50% contribution of the CN···HN bond, 30% of the CN···HC_{ph} interaction, and 20% of the $C_{ph}H$···OC interaction.

In the model shown in Figure 3, however, the relative position of molecules is slightly different from this lowest energy configuration, revealing the effect of the substrate periodicity in the positioning of molecules. The angle is closer to 43°, and the position of the CN group of 6DC atom is further away from the OC group of the DOA. Using this exact position of our model, we find a binding energy of 230 meV, to be compared with the 340 meV of the theoretical equilibrium position. To complete the picture, we find a cooperative effect of 40 meV per linkage, when two 2DCs (instead of just one) are connected to one DOA. This supplemental energy depends only to a minor extent on the exact position of 2DC and DOA molecules (theoretical equilibrium or experimental position) or on the number of phenyl rings in NC−Ph_X−CN molecules (2 and 3 tested). The binding energy holding together the bimolecular chain is thus evaluated to be ∼270 meV per bonding motif.

The second result shown in Figure 5b is related to the binding of two 6DC molecules perpendicular to each other (2DC with NC−Ph_4−CN (4DC) in our calculations). We find that the attractive zone for the carbonitrile group of the 2DC molecule runs all along the side of the 4DC molecule. However, the energetically most favorable sites are located in between the phenyl rings, with a preference for the end groups, exhibiting a maximal binding energy of 235 meV. At this position, the nitrogen is at a distance of 2.3 Å from both nearest hydrogen atoms. Two weak bonds seem to be participating in the link, partially explaining the particular shape of the energy map. The hopping energy barrier between neighboring sites along the 4DC molecule is found to be as weak as 45 meV (see Figure 5c). Finally, here again, the model shown in Figure 3 is slightly different from the theoretical equilibrium configuration shown in Figure 5b, both regarding the position and the size of the host molecule. The impact of the number of phenyl rings of the host molecule is found to be minimal, ∼10 meV. The change in position, however, causes a stronger decrease in the binding energy, yielding a final value of 185 meV (2DC connected to 6DC).

These two results confirm the observed larger strength of the $6DC_{ch}$−DOA bond over the $6DC_{ch}$−$6DC_{ru}$ bond. The translation of a singly linked $6DC_{ru}$ along the $6DC_{ch}$−DOA chains is addressed in Figure 5d. We computed the binding energy of one $2DC_{ru}$ in a large area covering the pathway from one $2DC_{ch}$ to the next, over a DOA. One can clearly see the saddle point at the junction of the $2DC_{ch}$ with the DOA. The binding energy at this point is found to be almost zero, yielding an energy barrier equal to the binding energy of the $6DC_{ch}$−$6DC_{ru}$ bond (185 meV). However, this hopping energy accounts only for one side of the $6DC_{ru}$ migration, and a more thorough consideration of the migration mechanism is essential to assert the combined effect of both sides. This investigation is presented in Figure 6.

In order to get an estimate of the effective hopping energy barrier for the migration of a $6DC_{ru}$ molecule from one stable position to the next, we tried to reconstruct the full interaction energy curve all along a likely migration path drawn from STM pictures (Figure 6b). This was achieved in four steps: (i) the whole migration path is decomposed into the step part and the straight part, and DFT simulations (notably Figure 5d) are used to determine the minimal energy path along *x* (Figure 6a). The hopping energy barrier between the minimal energy configurations around the step reaches 220 meV. (ii) The two parts of the interaction energy (step and straight part) are merged to get the full contribution of one $6DC_{ch}$−DOA chain to the migration energy curve (Figure 6c, plain line). (iii) The curve is mirrored to get the contribution of the other side's $6DC_{ch}$−DOA chain (Figure 6c, dashed line). The two curves are aligned along *x* so that the extremal stable positions coincide (dot dashed lines), as seen in the STM picture (Figure 6b). (iv) The two contributions are summed to get an estimate of the migration energy curve. The effective hopping energy barrier now reaches only 250 meV (and not two times 220 meV) because of the misalignment of the saddle point from both sides. This means that the saddle point exhibited in Figure 5d is not crossed simultaneously on both sides, but subsequently.

The calculated hopping energy for a strict translatory diffusion path is in fair agreement with our experimental findings from the Arrhenius analysis (hopping energy barrier of 205 meV) and fits even better when one considers the occurrence of the possible angular displacements of the $6DC_{ru}$ molecule as shown in the STM animation included in the Supporting Information. We indeed carried out a manipulation experiment at 10 K in which we pushed the $6DC_{ru}$ molecules along the chain direction. The images between each manipulation step are merged into a movie. Even though this mobility pathway is different from thermal excitation, the positions at which the $6DC_{ru}$ molecules reside after the manipulation process corroborate the presented scenario of guided molecular motion.

Anisotropic mobility is an important process in different nanosystems.[32] At the appropriate temperature, it governs the diffusion of metal adatoms,[39] resulting in the growth of 1D structures.[40] In a similar manner, small organic molecules[41] as well as their larger analogues[29,42−44] translate by this elementary process. In contrast to these systems, which rely on the anisotropic properties of the particular system, we create the

necessary 1D guides on an isotropic surface by hierarchic self-assembly of appropriately designed tectons. We have demonstrated that the diffusion of the mobile species is controlled by the interaction with the guides, which represents a novel approach to tailor molecular dynamics on surfaces in a universal fashion. Hierarchic assemblies may be generally useful to direct molecular motion *via* the tailored borders.

CONCLUSION

In summary, we have achieved the self-assembly of a hierarchic bimolecular network of the ladder-type in which, at temperatures exceeding ~70 K, 1D diffusion of large organic molecules takes place. Theoretic analysis clarifies that hierarchy is introduced into the chiral supramolecular structure by the energetics of the different bonds established between the two organic species, including a novel carbonitrile−oxalic amide motif. The dynamics of the mobile species is consistent with an Arrhenius-type of hopping and steered by the interaction with the ladder side rails. Our results demonstrate the usefulness of hierarchic design and reveal a new approach to guide molecular motion at nanostructured surfaces.

METHODS

The scanning tunneling microscopy (STM) experiments were performed using a home-built ultrahigh vacuum (base pressure 3×10^{-11} mbar) low-temperature STM. The Ag(111) substrate was prepared by repeated cycles of Ar^+ sputtering and annealing to 750 K to obtain flat terraces separated by monatomic steps. The two molecules, sexiphenyl dicarbonitrile (6DC) and *N*,*N*-diphenyl oxalic amide (DOA), were deposited from a double organic molecular beam epitaxy source with the quartz crucible at 572 and 467 K for 6DC and DOA, respectively, while keeping the substrate at 300 K. Both sequential and simultaneous deposition led to similar results. Following preparation, STM data were acquired at a substrate temperature (T_{sub}) as indicated, typically 10 K. The system's dynamics was probed in the range from 70 to 120 K.

For the theoretical investigation, we have used the projector-augmented wave approach as implemented in the ABINIT code,[45,46] within the local density approximation for the exchange-correlation energy. The cutoff energy used is 30 Ry. Since the code imposes periodic boundary conditions in all three directions, we ensured that the simulation box allowed a minimal distance of 8 Å between the molecules and their periodic images. We evaluated the subsequent error on total energy to be then lower than 10 meV. As molecules are rigidly displaced to obtain the energy maps, we checked the impact of geometrical relaxation on the binding energy by fully relaxing calculations for the lowest energy configurations, and we found energy differences lower than 10 meV. Also, for simplicity reasons, flat molecules were used in the calculations, whereas 6DC are known to present a tilting between the phenyl rings.[23,47] A test calculation involving two 2DC molecules revealed that impact on binding energy of the tilting is lower than 15 meV, despite the energy difference of almost 50 meV between tilted and untilted isolated 2DC molecule. The full energy maps displayed in Figure 5 are obtained using a Delaunay interpolation between the computed points.

Acknowledgment. Funding by the European Union *via* ERC Advanced Grant MolArt (°247299) and the German Research Foundation (DFG) through the TUM International Graduate School of Science and Engineering (IGSSE) and TUM Institute of Advanced Study (IAS) and the German Research Foundation (DFG) (BA 3395/2-1) and the Alexander von Humboldt Foundation are gratefully acknowledged.

Supporting Information Available: A movie made from a series of successive images showing the tip-induced diffusion of $6DC_{ru}$. Molecules were moved from the top-left to the bottom-right by pushing them approximately 3.5 nm (one network lattice constant) along direction A for a single manipulation event. A theoretical study of the impact of the Ag(111) substrate on the intermolecular bonding is also provided, which shows that the explicit inclusion of the substrate in DFT calculations is not essential to study intermolecular bonding occurring between physisorbed molecules, and can be emulated by the imposing coplanarity between them. This material is available free of charge *via* the Internet at http://pubs.acs.org.

REFERENCES AND NOTES

1. Lindsey, J. S. Self-Assembly in Synthetic Routes to Molecular Devices—Biological Principles and Chemical Perspectives—A Review. *New J. Chem.* **1991**, *15*, 153−−180.
2. Philp, D.; Stoddart, J. F. Self-Assembly in Natural and Unnatural Systems. *Angew. Chem., Int. Ed. Engl.* **1996**, *35*, 1155–1196.
3. Elemans, J. A. A. W.; Rowan, A. E.; Nolte, R. J. M. Mastering Molecular Matter. Supramolecular Architectures by Hierarchical Self-Assembly. *J. Mater. Chem.* **2003**, *13*, 2661–2670.
4. Barth, J. V.; Costantini, G.; Kern, K. Engineering Atomic and Molecular Nanostructures at Surfaces. *Nature* **2005**, *437*, 671–679.
5. De Feyter, S.; De Schryver, F. C. Two-Dimensional Supramolecular Self-Assembly Probed by Scanning Tunneling Microscopy. *Chem. Soc. Rev.* **2003**, *32*, 393–393.
6. Barth, J. V. Molecular Architectonic on Metal Surfaces. *Annu. Rev. Phys. Chem.* **2007**, *58*, 375–407.
7. Elemans, J.; Lei, S.; De Feyter, S. Molecular and Supramolecular Networks on Surfaces: From Two-Dimensional Crystal Engineering to Reactivity. *Angew. Chem., Int. Ed.* **2009**, *48*, 7298–7332.
8. Clair, S.; Pons, S.; Brune, H.; Kern, K.; Barth, J. V. Mesoscopic Metallosupramolecular Texturing by Hierarchic Assembly. *Angew. Chem., Int. Ed.* **2005**, *44*, 7294–7297.
9. Blüm, M.-C.; Ćavar, E.; Pivetta, M.; Patthey, F.; Schneider, W.-D. Conservation of Chirality in a Hierarchical Supramolecular Self-Assembled Structure with Pentagonal Symmetry. *Angew. Chem., Int. Ed.* **2005**, *44*, 5334–5337.
10. Otero, R.; Schöck, M.; Molina, L. M.; Laegsgaard, E.; Stensgaard, I.; Hammer, B.; Besenbacher, F. Guanine Quartet Networks Stabilized by Cooperative Hydrogen Bonds. *Angew. Chem., Int. Ed.* **2005**, *44*, 2270–2275.
11. Staniec, P. A.; Perdigao, L. M. A.; Saywell, A.; Champness, N. R.; Beton, P. H. Hierarchical Organisation on a Two-Dimensional Supramolecular Network. *ChemPhysChem* **2007**, *8*, 2177–2181.
12. Schlickum, U.; Decker, R.; Klappenberger, F.; Zoppellaro, G.; Klyatskaya, S.; Auwärter, W.; Neppl, S.; Kern, K.; Brune, H.; Ruben, M.; *et al.* Chiral Kagomé Lattice from Simple Ditopic Molecular Bricks. *J. Am. Chem. Soc.* **2008**, *130*, 11778–11782.
13. Ruben, M.; Ziener, U.; Lehn, J. M.; Ksenofontov, V.; Gutlich, P.; Vaughan, G. B. M. Hierarchical Self-Assembly of Supramolecular Spintronic Modules into 1D- and 2D-Architectures with Emergence of Magnetic Properties. *Chem.—Eur. J.* **2005**, *11*, 94–100.
14. Spillmann, H.; Dmitriev, A.; Lin, N.; Messina, P.; Barth, J. V.; Kern, K. Hierarchical Assembly of Two-Dimensional

Homochiral Nanocavity Arrays. *J. Am. Chem. Soc.* **2003**, *125*, 10725–10728.
15. Meier, C.; Landfester, K.; Kunzel, D.; Markert, T.; Gross, A.; Ziener, U. Hierarchically Self-Assembled Host–Guest Network at the Solid–Liquid Interface for Single-Molecule Manipulation. *Angew. Chem., Int. Ed.* **2008**, *47*, 3821–3825.
16. de Wild, M.; Berner, S.; Suzuki, H.; Yanagi, H.; Schlettwein, D.; Ivan, S.; Baratoff, A.; Guentherodt, H. J.; Jung, T. A. A Novel Route to Molecular Self-assembly: Self-Intermixed Monolayer Phases. *ChemPhysChem* **2002**, *3*, 881–885.
17. Ruiz-Osés, M.; González-Lakunza, N.; Silanes, I.; Gourdon, A.; Arnau, A.; Ortega, J. E. Self-Assembly of Heterogeneous Supramolecular Structures with Uniaxial Anisotropy. *J. Phys. Chem. B* **2006**, *110*, 25573–25577.
18. Theobald, J. A.; Oxtoby, N. S.; Phillips, M. A.; Champness, N. R.; Beton, P. H. Controlling Molecular Deposition and Layer Structure with Supramolecular Surface Assemblies. *Nature* **2003**, *424*, 1029–1031.
19. Cañas-Ventura, M. E.; Xiao, W.; Wasserfallen, D.; Müllen, K.; Brune, H.; Barth, J. V.; Fasel, R. Self-Assembly of Periodic Bicomponent Wires and Ribbons. *Angew. Chem., Int. Ed.* **2007**, *46*, 1814–1818.
20. Barrena, E.; de Oteyza, D. G.; Dosch, H.; Wakayama, Y. 2D Supramolecular Self-Assembly of Binary Organic Monolayers. *ChemPhysChem* **2007**, *8*, 1915–1918.
21. Hipps, K. W.; Scudiero, L.; Barlow, D. E.; Cooke, M. P. A Self-Organized 2-Dimensional Bifunctional Structure Formed by Supramolecular Design. *J. Am. Chem. Soc.* **2002**, *124*, 2126–2127.
22. Klappenberger, F.; Cañas-Ventura, M. E.; Clair, S.; Pons, S.; Schlickum, U.; Qu, Z. R.; Strunskus, T.; Comisso, A.; Wöll, C.; Brune, H.; *et al.* Does the Surface Matter? Hydrogen Bonded Chain Formation of an Oxalic Amide Derivative in Two and Three Dimensional Environment. *ChemPhysChem* **2008**, *9*, 2522–2530.
23. Kühne, D.; Klappenberger, F.; Decker, R.; Schlickum, U.; Brune, H.; Klyatskaya, S.; Ruben, M.; Barth, J. V. Self-Assembly of Nanoporous Chiral Networks with Varying Symmetry from Sexiphenyl-Dicarbonitrile on Ag(111). *J. Phys. Chem. C* **2009**, *113*, 17851–17859.
24. Krenner, W.; Klappenberger, F.; Kühne, D.; Diller, K.; Qu, Z.-R.; Ruben, M.; Barth, J. V. Positioning of Single Co Atoms Steered by a Self-Assembled Organic Molecular Template. *J. Phys. Chem. Lett.* **2011**, *2*, 1639–1645.
25. Klappenberger, F.; Kühne, D.; Krenner, W.; Silanes, I.; Arnau, A.; Garcia de Abajo, F. J.; Klyatskaya, S.; Ruben, M.; Barth, J. V. Dichotomous Array of Chiral Quantum Corrals by a Self-Assembled Nanoporous Kagome Network. *Nano Lett.* **2009**, *9*, 3509–3514.
26. Henningsen, N.; Rurali, R.; Franke, K. J.; Fernández-Torrente, I.; Pascual, J. I. Trans to Cis Isomerization of an Azobenzene Derivative on a Cu(100) Surface. *Appl. Phys. A: Mater. Sci. Process.* **2008**, *93*, 241–246.
27. Böhringer, M.; Morgenstern, K.; Schneider, W. D.; Berndt, R.; Mauri, F.; De Vita, A.; Car, R. Two-Dimensional Self-Assembly of Supramolecular Clusters and Chains. *Phys. Rev. Lett.* **1999**, *83*, 324–327.
28. Dmitriev, A.; Lin, N.; Weckesser, J.; Barth, J. V.; Kern, K. Supramolecular Assemblies of Trimesic Acid on a Cu(100) Surface. *J. Phys. Chem. B* **2002**, *106*, 6907–6912.
29. Weckesser, J.; Barth, J. V.; Kern, K. Direct Observation of Surface Diffusion of Large Organic Molecules at Metal Surfaces: PVBA on Pd(110). *J. Chem. Phys.* **1999**, *110*, 5351–5354.
30. Cañas-Ventura, M. E.; Klappenberger, F.; Clair, S.; Pons, S.; Kern, K.; Brune, H.; Strunskus, T.; Wöll, C.; Fasel, R.; Barth, J. V. Coexistence of One- and Two-Dimensional Supramolecular Assemblies of Terephthalic Acid on Pd(111) Due to Self-Limiting Deprotonation. *J. Chem. Phys.* **2006**, *125*, 184710.
31. Kühne, D.; Klappenberger, F.; Krenner, W.; Klyatskaya, S.; Ruben, M.; Barth, V. J. Rotational and Constitutional Dynamics of Caged Supramolecules. *Proc. Natl. Acad. Sci. U.S.A.* **2010**, *50*, 21332–21336.
32. Barth, J. V. Transport of adsorbates at metal surfaces: From thermal migration to hot precursors. *Surf. Sci. Rep.* **2000**, *40*, 75–149.
33. Barth, J. V.; Weckesser, J.; Cai, C.; Günter, P.; Bürgi, L.; Jeandupeux, O.; Kern, K. Building Supramolecular Nanostructures at Surfaces by Hydrogen Bonding. *Angew. Chem., Int. Ed.* **2000**, *39*, 1230–1234.
34. Schiffrin, A.; Riemann, A.; Auwärter, W.; Pennec, Y.; Weber-Bargioni, A.; Cvetko, D.; Cossaro, A.; Morgante, A.; Barth, J. V. Zwitterionic Self-Assembly of l-Methionine Nanogratings on the Ag(111) Surface. *Proc. Natl. Acad. Sci. U.S.A.* **2007**, *104*, 5279–5284.
35. Schiffrin, A.; Reichert, J.; Auwärter, W.; Jahnz, G.; Pennec, Y.; Weber-Bargioni, A.; Stepanyuk, V. S.; Niebergall, L.; Bruno, P.; Barth, J. V. Self-Aligning Atomic Strings in Surface-Supported Biomolecular Gratings. *Phys. Rev. B* **2008**, *78*, 035424.
36. Weckesser, J.; De Vita, A.; Barth, J. V.; Cai, C.; Kern, K. Mesoscopic Correlation of Supramolecular Chirality in One-Dimensional Hydrogen-Bonded Assemblies. *Phys. Rev. Lett.* **2001**, *87*, 096101.
37. Barth, J. V.; Weckesser, J.; Trimarchi, G.; Vladimirova, M.; De Vita, A.; Cai, C.; Brune, H.; Günter, P.; Kern, K. Stereochemical Effects in Supramolecular Self-Assembly at Surfaces: 1-D *versus* 2-D Enantiomorphic Ordering for PVBA and PEBA on Ag(111). *J. Am. Chem. Soc.* **2002**, *124*, 7991–8000.
38. A complete analysis will be presented in a forthcoming paper.
39. Senft, D. C.; Ehrlich, G. Long Jumps in the Surface-Diffusion: One-Dimensional Migration of Isolated Adatoms. *Phys. Rev. Lett.* **1995**, *74*, 294–297.
40. Röder, H.; Hahn, E.; Brune, H.; Bucher, J. P.; Kern, K. Building One-Dimensional and 2-Dimensional Nanostructures by Diffusion-Controlled Aggregation at Surfaces. *Nature* **1993**, *366*, 141–143.
41. Briner, B. G.; Doering, M.; Rust, H.-P.; Bradshaw, A. M. Microscopic Molecular Diffusion Enhanced by Adsorbate Interactions. *Science* **1997**, *278*, 257–260.
42. Schunack, M.; Linderoth, T. R.; Rosei, F.; Laegsgaard, E.; Stensgaard, I.; Besenbacher, F. Long Jumps in the Surface Diffusion of Large Molecules. *Phys. Rev. Lett.* **2002**, *88*, 156102.
43. Kwon, K.-Y.; Wong, K. L.; Pawin, G.; Bartels, L.; Stolbov, S.; Rahman, T. S. Unidirectional Adsorbate Motion on a High-Symmetry Surface: "Walking" Molecules Can Stay the Course. *Phys. Rev. Lett.* **2005**, *95*, 166101.
44. Weckesser, J.; Barth, J. V.; Kern, K. Mobility and Bonding Transition of C_{60} on Pd(110). *Phys. Rev. B* **2001**, *64*, 161403.
45. Gonze, X.; Rignanese, G.-M.; Verstraete, M.; Beuken, J.-M.; Pouillon, Y.; Caracas, R.; Jollet, F.; Torrent, M.; Zerah, G.; Mikami, M.; *et al.* A Brief Introduction to the ABINIT Software Package. *Z. Kristallogr.* **2005**, *220*, 558–562.
46. Torrent, M.; Jollet, F.; Bottin, F.; Zerah, G.; Gonze, X. Implementation of the Projector Augmented-Wave Method in the ABINIT Code. Application to the Study of Iron Under Pressure. *Comput. Mater. Sci.* **2008**, *42*, 337–351.
47. Klappenberger, F.; Kühne, D.; Marschall, M.; Neppl, S.; Krenner, W.; Nefedov, A.; Strunskus, T.; Fink, K.; Wöll, C.; Klyatskaya, S.; *et al.* Uniform π-System Alignment in Thin Films of Template-Grown Dicarbonitrile-Oligophenyls. *Adv. Funct. Mater.* **2011**, *21*, 1631–1642.